https://doi.org/10.5194/acp-2020-330
Preprint. Discussion started: 29 April 2020

Atmospheric Chemistry and Physics Discussions

Pre-deliquescent water uptake in deposited nanoparticles observed with *in situ* ambient pressure X-ray photoelectron spectroscopy

Jack J. Lin[1], Kamal Raj R Mundoli[1], Stella Wang[2], Esko Kokkonen[3], Mikko-Heikki Mikkelä[3], Samuli Urpelainen[1], and Nønne L. Prisle[1]

[1]Nano and Molecular Systems Research Unit, P. O. Box 3000, FI-90014 University of Oulu, Finland
[2]Division of Physics, Math, and Astronomy, California Institute of Technology, Pasadena, California, 91125, USA
[3]MAX IV Laboratory, Lund University, Box 118, SE-22100 Lund, Sweden

Correspondence: Samuli Urpelainen (samuli.urpelainen@oulu.fi); Nønne L. Prisle (nonne.prisle@oulu.fi)

Abstract. We study the adsorption of water onto deposited inorganic sodium chloride and organic malonic acid and sucrose nanoparticles at ambient water pressures corresponding to relative humidities (RH) from 0 to 16%. To obtain information about water uptake at conditions where not accessible with typical aerosol instrumentation, we use surface-sensitive ambient pressure X-ray photoelectron spectroscopy (APXPS), which has a detection sensitivity from parts per thousand. Our results show that water is already adsorbed on sodium chloride particles at RH well below deliquescence, and that the chemical environment on the particle surface is changing with increasing humidity. While the sucrose particles exhibit only very modest changes on the surface at these relative humidities, the chemical composition and environment of malonic acid particle surfaces is clearly affected. Our observations indicate that water uptake by inorganic and organic aerosol particles could already have an impact on atmospheric chemistry at low relative humidities. We also conclude that the APXPS technique is a viable tool for studying chemical changes on the surfaces of atmospherically relevant aerosol particles which are not accessible with typical online mass- and volume-based methods.

1 Introduction

The interaction between atmospheric particulate matter and water is one of the most important processes in Earth's atmosphere. The amount of water associated with an aerosol particle is a function of its intrinsic hygroscopicity and the ambient relative humidity (RH). Liquid water comprises a significant fraction of the global aerosol mass with field measurements documenting the global presence of the metastable aerosol phase state (Rood et al., 1989; Nguyen et al., 2016). Condensed water in the atmosphere critically influences both direct and indirect climate effects of aerosols, governed by aerosol growth and light scattering and via the activation of aerosol particles into cloud droplets (Kreidenweis and Asa-Awuku, 2014). The adsorption of water onto aerosol particles has the ability to affect atmospheric chemistry as a source of secondary organic aerosol (McNeill, 2015), via the mobilization of ions (Cwiertny et al., 2008), changing acid/base equilibrium (Freedman et al., 2018), or by

https://doi.org/10.5194/acp-2020-330
Preprint. Discussion started: 29 April 2020


Atmospheric Chemistry and Physics Discussions

enhancing photochemistry (Herrmann et al., 2010). Uptake of water to the aerosol phase also determines the environment for surface, bulk and multiphase chemistry with implications for air quality, climate and the hydrological cycle (Prisle et al., 2012; Boucher et al., 2013).

A wide range of experimental techniques are available to study the hygroscopic properties of particles in sub-saturated (< 100% RH) conditions, including humidity-tandem differential mobility analyzers (H-TDMA), various optical extinction and scattering methods, physisorption analyzers, quartz crystal microbalances and various microscopic and spectroscopic methods (Kreidenweis and Asa-Awuku, 2014; Tang et al., 2019). The drawback of many of the otherwise highly valuable traditional aerosol techniques, such as the H-TDMA or optical methods, is that they are based on detection of growth in mass or volume. Because of this, they are not sensitive enough when applied alone for detecting minute amounts of water adsorbed onto the aerosols at low humidity or below the deliquescence relative humidity (DRH). Furthermore, most of these methods are insensitive to surface-specific chemistry and the phase state of adsorbed water and do not provide molecular-level information about the system. This can lead to underestimating the amount and impact of water adsorption at lower RH. The equilibrium between water and the particle phase has been shown experimentally to depend on the particle phase state and humidity history, with important implications for particle hygroscopic growth and cloud droplet activation (Bilde and Svenningsson, 2004).

A number of spectroscopic techniques have been applied to systems of environmental and atmospheric relevance (Ault and Axson, 2016; Tang et al., 2019). Surface-sensitive techniques such as X-ray photoelectron spectroscopy (XPS) provide molecular-level information on the chemical composition and properties of surfaces. So far, most of these studies, in particular those employing XPS, have adopted a surface science approach using the simplified case of single crystal surfaces as an important first step (Tang et al., 2019). For example, XPS has been used to study the photochemistry of TiO_2(110) (Lampimäki et al., 2015), ionic mobility on NaCl (001) surfaces induced by water adsorption (Verdaguer et al., 2008) and reaction of water vapor with MgO (001) surfaces (Newberg et al., 2011). XPS on a liquid micro-jet (Winter, 2009) has also been used to study surface-specific chemistry of aqueous solutions comprising atmospherically relevant organic surfactants (Prisle et al., 2012; Werner et al., 2014; Walz et al., 2015, 2016; Toribio et al., 2018; Werner et al., 2018; Ammann et al., 2018) as model systems for atmospheric water droplets. Experiments on single aerosol particles are, on the other hand, scarce (Antonsson et al., 2015; Shakya et al., 2016; Ouf et al., 2016). As some of the few examples of atmospheric relevance, we have previously studied solvation of RbBr in free flying water clusters (Hautala et al., 2017b), as well as size-dependent structural phase changes in CsBr, as a model system for salt clusters of higher environmental relevance (Hautala et al., 2017a). With the advent of high-brilliance synchrotron radiation and recent developments in electron analyzer technology, previous barriers of too low sample density can be overcome, enabling XPS studies under realistic conditions, *in situ* and *operando*, using the so-called ambient pressure XPS (APXPS) technique (Salmeron and Schlögl, 2008; Ogletree et al., 2009; Starr et al., 2013; Kong et al., 2020).

In this work, we study the pre-deliquescent water uptake of laboratory-generated, deposited sodium chloride (NaCl), malonic acid, and sucrose particles. NaCl is a major component of sea salt, the most abundant aerosol species by mass in the atmosphere (Murphy et al., 2019). Salt aerosols, apart from being important light scatterers, also take part in atmospheric chemistry by interacting with atmospheric trace gases as a source of halogens (Rossi, 2003), especially in the presence of water in the aerosols. The water uptake and deliquescence of salt aerosol particles can be affected by the presence of other inorganic

https://doi.org/10.5194/acp-2020-330
Preprint. Discussion started: 29 April 2020


Atmospheric Chemistry and Physics Discussions

or organic matter. For example, the presence of malonic acid in NaCl aerosol will not only lower the DRH of the aerosol, but also facilitate the depletion of chlorine (Laskin et al., 2012). Organic material comprises a large fraction of the ambient aerosol mass (Kanakidou et al., 2005), and malonic acid and sucrose represent hygroscopic organic compounds with different chemical functionalities. Dicarboxylic acids such as malonic acid have been identified in ambient aerosols samples where they can dominate the water-soluble organic fraction (Khwaja, 1995; Yu et al., 2005; Decesari et al., 2000, 2001) and are hygroscopic in both sub and supersaturated conditions (Prenni et al., 2001; Hori et al., 2003; Rissman et al., 2007; Pope et al., 2010). Sucrose is studied as a model carbohydrate that can form a glassy state in response to changing relative humidity with effects on its ability to act as either cloud or ice nuclei (Zobrist et al., 2011; Estillore et al., 2017). Utilizing APXPS, interaction with water vapor at the particle surface was studied at relative humidities between 0 and 16%. To the best of our knowledge, this is the first time XPS has been used on sampled nano-scale particles of immediate atmospherically relevant composition at ambient pressure conditions.

2 Experimental

We employed the APXPS technique to obtain chemically-specific information about the composition of the nanoparticle surfaces. XPS is a surface-sensitive technique, where the first few nanometers of a sample are probed by measuring the intensity of photoelectrons emitted from a sample as a function of the electron kinetic energy (E_k). When the ionizing photon energy ($h\nu$) is known, the binding energy (E_b) can be determined simply as $E_b = h\nu - E_k$. In addition to the binding energy, peak areas are also determined. Spectral fitting techniques are employed to obtain accurate results for both binding energies and peak areas. Together, these parameters give information about the chemical composition and environment (binding energy) and relative abundances of elements (peak area) on the surface of the sample.

Experiments were carried out at the APXPS end station (Schnadt et al., 2012; Knudsen et al., 2016) of the SPECIES beamline (Urpelainen et al., 2017) at the MAX IV Laboratory in Lund, Sweden. The end station is equipped with a hemispherical SPECS Phoibos NAP-150 electron energy analyzer and allows for measurements both at ultra-high vacuum (UHV) conditions, as well as up to 25 mbar in an ambient pressure (AP) cell. During the experiments, the SPECIES beamline was still under construction, and we used a double anode (SPECS XR-50) X-ray source with Al (1486.6 eV) and Mg (1253.6 eV) anodes for exciting the samples instead of synchrotron radiation.

Samples were prepared at the Lund University Aerosol Lab and deposited on silicon and gold substrates. Deposited samples were kept and transferred to the SPECIES end station in a desiccator in order not to expose them to ambient humidity for extended periods of time prior to the experiments. For the XPS measurements, substrates were mounted onto stainless steel sample holders using an adhesive Cu tape in a clean tent environment and loaded into the end station. The experiments consisted of recording C 1s, O 1s (sucrose and malonic acid), Na 1s and Cl 2p (NaCl) core level XPS spectra of the deposited aerosol particles at UHV and *in situ* at varying RH conditions. The Al anode was used to measure spectra from NaCl while the Mg anode was used to measure spectra from the malonic acid and sucrose samples.

A detailed account of the sample preparation process and experimental conditions is given in the following sections.

https://doi.org/10.5194/acp-2020-330
Preprint. Discussion started: 29 April 2020

Atmospheric Chemistry and Physics Discussions

2.1 Sample preparation

Aerosol samples were generated by nebulizing aqueous solutions of sodium chloride ($NaCl$), sucrose ($C_{12}H_{22}O_{11}$), and malonic acid ($CH_2(COOH)_2$). Solutions were prepared using ultra-pure Milli-Q water. All chemicals were obtained from Sigma-Aldrich and used without further treatment.

The air flow containing solution droplets (3 L min^{-1}) was mixed with dry, particle-free air (3 L min^{-1}) in a 3 L aerosol mixing chamber. From the mixing chamber, 1–1.5 L min^{-1} was sent through a diffusion dryer followed by a ^{63}Ni bipolar charger. The dried and charge neutralized aerosol flow was divided between a scanning mobility particle sizer (SMPS; TSI 3936) for size distribution characterization and a nanometer aerosol sampler (NAS; TSI 3089) for sample collection of the entire dry aerosol particle size distribution. Sodium chloride particles were collected onto silicon (with native oxide) wafers, while sucrose and malonic acid particles were deposited onto a gold film substrate.

The surface coverage on the substrate in the ESP is a function of the particle concentration in the gas flow, the drift velocity of the particles in the electric field, and the total sampling time (Preger et al., 2020). Particles are assumed to be spherical across the entire size distribution with a charge distribution described by Boltzmann statistics. We further assume 100% deposition efficiency of the positively charged fraction and uniform with coverage with values above 100% indicating the presence of more than one monolayer of deposited particles. Details of the sample generation are given in Table 1.

Table 1. Aerosol sampling data including generated size distribution information and sample collection parameters.

Compound	Mean Size Distribution				Sample Collection			
	μ_N (nm)	σ_g	N (cm^{-1})	μ_{SA} (nm^2)	Q (L min^{-1})	t (min)	Substrate	Coverage (%)
Sodium chloride	72	2.0	3.94×10^5	195	1.1	42	Si	232
Sucrose	79	2.2	3.59×10^4	202	1.1	90	Au	56
Malonic acid	52	2.1	1.02×10^5	193	1.2	275	Au	245

2.2 XPS measurements

UHV XPS spectra were recorded using a pass energy of 50 eV and an entrance slit of 3 mm × 20 mm. This contributes to an experimental broadening of approximately 500 meV in addition to the natural broadening from the excitation source (850 meV for Al K_α and 680 meV for Mg K_α radiation).

For measurements at humid conditions, samples were transferred from the UHV manipulator to the AP cell. Milli-Q water vapor was let into the AP cell through a high precision leak valve. The pressure inside the cell was kept constant using a valve connected to a pump in a feedback loop with an absolute capacitance manometer. All measurements were made at 25 °C at which the saturation vapor pressure of water is P_{sat} = 31.73 mbar. The relative humidity was calculated using the (water) vapor pressure inside the AP cell so that RH = P_{cell}/P_{sat}. While samples were inside the cell, spectra were recorded at different water vapor pressure conditions (NaCl: 0, 2, 5, and again at 0 mbar; sucrose 0.2, 1, and 5 mbar; malonic acid 0.2 and 1 mbar). The water vapor pressures of 0, 0.2, 1, 2, and 5 mbar correspond to relative humidities of 0, 0.63, 3.2, 6.3, and 16%, respectively.

https://doi.org/10.5194/acp-2020-330
Preprint. Discussion started: 29 April 2020


Atmospheric Chemistry and Physics Discussions

These relative humidities are well below the DRH for NaCl (75.3% (Tang and Munkelwitz, 1993)), malonic acid (72.1% (Parsons et al., 2004)), and sucrose (85.7% (Yao et al., 2011)). Any remaining air was removed from the water by several freeze-pump-thaw cycles before introducing the vapor into the AP cell. The cell was also purged with dry nitrogen gas in order to remove any excess water after the experiment. In the case of NaCl particles, the sample was heated up to 125 °C using a button heater placed behind the sample holder. This was done after the sample was dosed up to 10 mbar to see if the changes incurred on exposure to water vapor were reversible. Spectra obtained at 10 mbar, however, are not included in the analysis below due to very low signal to noise ratios.

The electron count rates inside the AP cell are reduced when compared to measurements in UHV conditions due to the attenuation of X-ray intensity by the SiN_3/Al window, the limited aperture of the differential pumping of the electron analyzer and scattering of the photoelectrons from the vapor (Knudsen et al., 2016). In order to increase the count rates, spectra recorded inside the cell were acquired at a pass energy of 100 eV instead of 50 eV as used in UHV conditions in order to compensate for the reduced intensity. The analyzer broadening when using 100 eV pass energy was approximately 1.00 eV. Each spectrum was recorded 50-100 times in static conditions for increased statistics and averaged in time for the final representation.

2.3 Data Analysis

Recorded XPS spectra were fitted in order to accurately determine the binding energies of the core electrons and the relative amounts (by determining corresponding XPS peak areas) of elements under different conditions. Data analysis was performed using Igor Pro (WaveMetrics, Inc, Lake Oswego, OR, USA). A Shirley-type background was removed from the data before fitting the peaks using the SPANCF curve fitting macro package (Kukk et al., 2001, 2005). All spectra were fitted using symmetric Voigt line shapes. A linear background was included in all the fits to remove any residual background after the Shirley-type background removal. The energy scales of the spectra were calibrated using the well known values of Si 2p and Au 4f for the silicon and gold substrates, as the low aerosol particle coverage allowed simultaneous measurement of the substrate.

We determine the elemental composition of particle surfaces as the relative ratios of the core level peak areas. Before extracting relative ratios of the peaks, all spectra were normalized to the photoionization cross section (Yeh and Lindau, 1985) of the given core electron and attenuation due to scattering of the photoelectrons from the water vapor. The attenuation must be taken into account, because the fixed excitation energy from the X-ray source leads to significantly different kinetic energies of the emitted photoelectrons and consequently different mean free paths in the vapor environment. The attenuation of photoelectron intensity was estimated by using the kinetic theory formulation (Ogletree et al., 2009) and measured electron scattering cross section data (Muñoz et al., 2007).

3 Results and discussion

Below we present experimental XPS spectra together with details and results of curve fitting for deposited NaCl, sucrose and malonic acid nanoparticles. Binding energy shifts of varying degree from the dry conditions are observed with increasing rela-

https://doi.org/10.5194/acp-2020-330
Preprint. Discussion started: 29 April 2020


Atmospheric Chemistry and Physics Discussions

tive humidity, indicating changes in the chemical environment of the target element. In addition, changes in the stoichiometry of molecules on the particle surface can be seen from the intensity ratios between different core level XPS peaks. This is a sign of changes in the chemical composition on the surface of the aerosol particles. These observations are clear indications that water is already being adsorbed onto the particles and interacting with molecules on their surfaces at these low relative humidity conditions. The implications and possible interpretations of these observations are discussed below.

3.1 NaCl

Figures 1 and 2 show the recorded Na 1s and Cl 2p spectra of NaCl aerosol particles deposited on a Si substrate measured at 0, 2, 5, and again at 0 mbar (0, 6.3, 16, and 0% RH, respectively) water vapor pressure. Spectra recorded at UHV have been omitted from the figures since they are redundant with the measurements made in the AP chamber at 0 mbar water vapor pressure. The Na 1s spectra were fitted using a single, symmetric Voigt peak, except for the 0 mbar spectrum after water exposure, where two peaks were required in order to obtain a fit that represents the measured spectrum. The Cl 2p spectra were fitted with two peaks representing the two spin-orbit components. The O 1s region for the NaCl sample was also monitored during the experiments, but the spectra are dominated with the signals from the native oxide of the Si wafer and the vapor phase water, and no direct signs of adsorbed or liquid water could be seen in the spectra at these low RH. These spectra are therefore omitted from the discussion below.

After calibrating the energy scale using the substrate Si 2p peaks as described earlier, the binding energy of the Na 1s core level at UHV conditions was determined to be 1073.48 eV and is indicated by the dashed vertical line in Fig. 1. The signal-to-noise ratio in the spectra recorded at 5 mbar (16% RH) is very low and the fitted line should be regarded more as guiding the eye than an accurate fit to the peak. The binding energy of the Cl 2p 3/2 component at UHV conditions was determined to be 200.3 eV shown by the dashed vertical line in Fig. 2.

Figure 3 shows the binding energy shifts of the Na 1s and Cl 2p core level peaks (red diamonds and dots, respectively) as a function of water vapor pressure at 25 °C. We observe a significant shift of approximately 1.1 eV in both Na 1s and Cl 2p binding energies already when water vapor is introduced into the system at very low relative humidities. After this first rapid decrease, the Cl 2p binding energies reach a plateau, when the relative humidity is increased to 16%. The binding energy shifts for Na 1s and Cl 2p between 0% and 6.3% RH are nearly identical, but the subsequent shift for Na 1s between 6.3% and 16% RH is towards larger binding energies by 0.17 eV, while Cl 2p shifts towards lower binding energies by -0.26 eV. The binding energy shifts observed here are in good agreement with those reported for Na 2s and Cl 2p in NaCl (001) single crystal surfaces by Verdaguer et al. (2008) showing even a similar plateau at intermediate pressures. As they did not report the magnitude of the binding energy shift from 0 to 5% RH, we have shifted the 5% RH data point of Verdaguer et al. (2008) to coincide with our data in Fig. 3 for easier qualitative comparison of the two. The shift of the Na 1s peak for deposited aerosol in the present work towards larger binding energies at 16% RH is not entirely in line with the observations on NaCl (001), which show a monotonic shifts towards lower binding energies both for Na 2s and Cl 2p peaks. However, the poorer quality of the experimental spectrum for aerosol Na 1s at 16% RH in the present work, compared to spectra recorded at lower RH, leads to larger uncertainty in the peak fitting procedure. Furthermore, the shifts observed for NaCl nanoparticles in the present work

https://doi.org/10.5194/acp-2020-330
Preprint. Discussion started: 29 April 2020

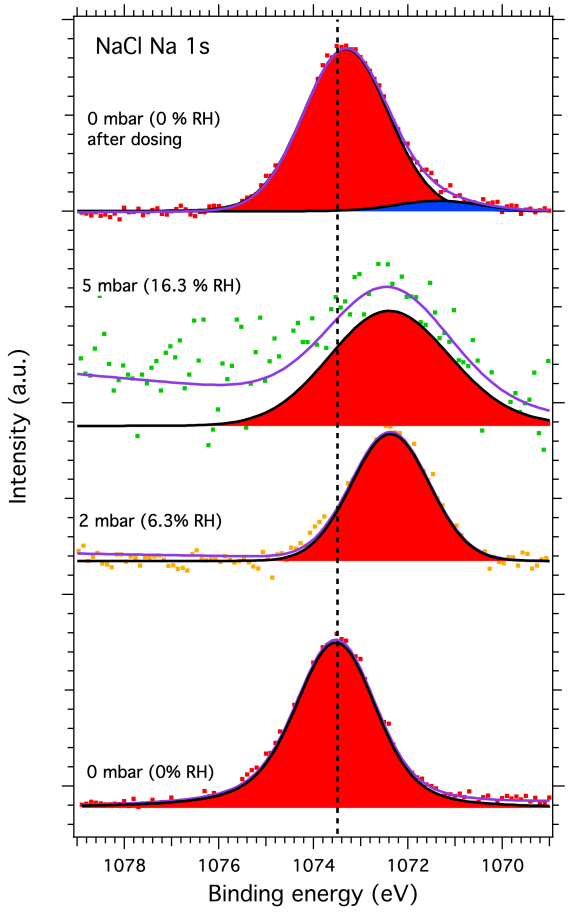

Figure 1. Na 1s XPS spectra of NaCl aerosol particles recorded at different water vapor pressures (relative humidities, RH). The dots show the recorded data, the solid lines the fit envelope curve and the red and blue peaks the fitted Voigt profiles. The dashed vertical line shows the binding energy of Na 1s at 0 mbar pressure (0% RH) at the beginning of the experiments. Photon energy was 1486.6 eV from the Al anode.

are larger for Cl 2p than for Na 1s, as opposed to larger shifts (by approximately 50 meV) for Na 2s than Cl 2p in the NaCl (001) single crystal. In our experiments, the water vapor was removed from the AP cell after the measurements at 16% RH and another spectrum was recorded at 0% RH. We see that when RH decreases from 16% to 0%, the binding energies of the Na 1s and Cl 2p do not shift back to their original values, but a memory effect of approximately 0.2 eV for both Na 1s and Cl 2p is observed. This is in line with the observations by Verdaguer et al. (2008) who also report a memory effect of less than 0.5 eV for single crystal NaCl.

In addition to the shifts in binding energies, we also investigated the effects of water vapor on the width of the XPS peaks, which can indicate changes in the chemical environment or charge carrier mobility on the aerosol surfaces. However, while we found clear binding energy shifts (Fig. 3), we did not observe any significant changes in the peak width of either the Na 1s or the Cl 2p peaks. In contrast, the data obtained by Verdaguer et al. (2008) show decreasing total widths of Na 2s

https://doi.org/10.5194/acp-2020-330
Preprint. Discussion started: 29 April 2020

Atmospheric Chemistry and Physics Discussions

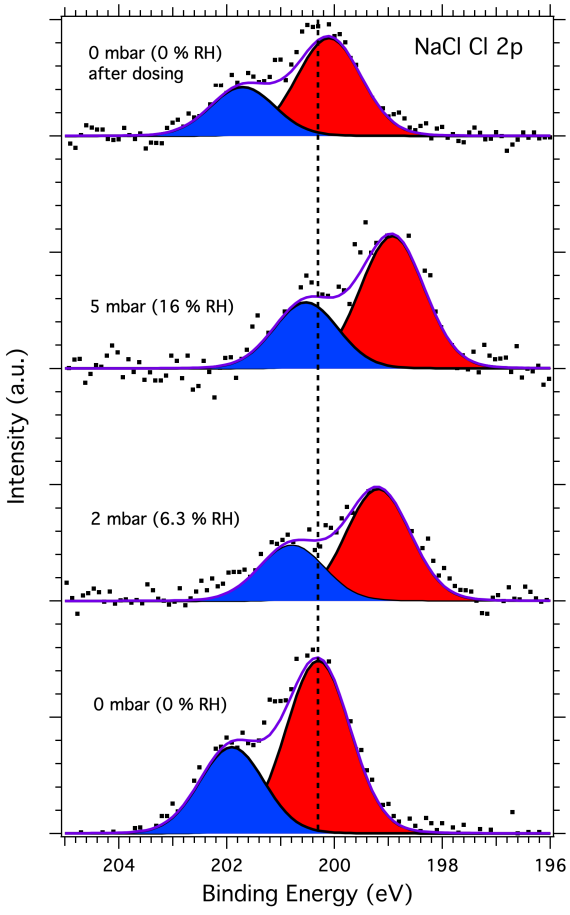

Figure 2. Cl 2p XPS spectra of NaCl aerosol particles recorded at different water vapor pressures (relative humidities, RH). The dots show the recorded data, the solid lines the fit envelope curve and the red and blue peaks the fitted 3/2 and 1/2 spin-orbit components, respectively. The dashed vertical line shows the binding energy of Cl 2p 3/2 component at 0 mbar pressure (0% RH) at the beginning of the experiments. Photon energy was 1486.6 eV from the Al anode.

and Cl 2p peaks for NaCl (001) single crystal with increasing relative humidity, following qualitatively the behavior of their observed core level binding energy shifts. The difference between deposited aerosols and single crystal spectra may, at least partially, be explained by the experimental resolution, which is lower in the present study with peak widths dominated by
195 experimental factors. In the NaCl (001) case, the observed binding energy shifts are attributed to the discharging of the surface, where increasing relative humidity causes the surface to be gradually discharged due to ionized water vapor and secondary electrons. As water is adsorbed onto the surface, it leads to solvation of surface ions and increased mobility of these charge carriers. This ion mobility makes discharging more efficient, leading to further shifts in observed binding energies. According to Verdaguer et al. (2008) these solvation effects become more significant above approximately 35% RH. This interpretation
200 is further supported by scanning force microscopy studies and infrared studies that show modifications in the surface structure

https://doi.org/10.5194/acp-2020-330
Preprint. Discussion started: 29 April 2020

Atmospheric Chemistry and Physics Discussions

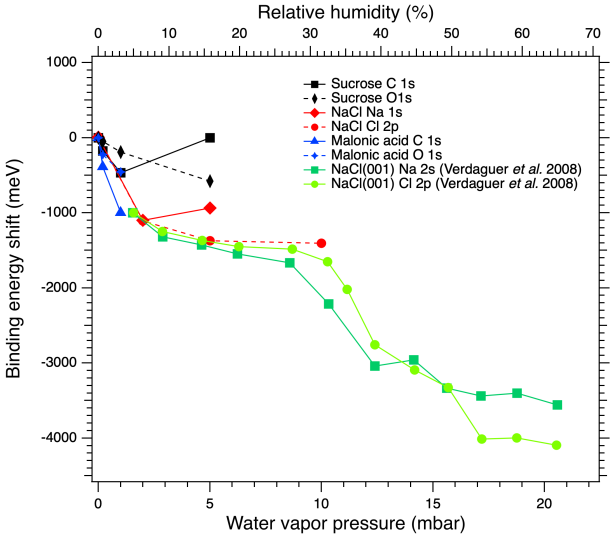

Figure 3. Binding energy shifts of the core level peaks for NaCl, sucrose and malonic acid particles, as functions of water vapor pressure (relative humidity). The green/light green plots extending above 60% RH show the data from Verdaguer et al. (2008) for single NaCl crystal that has been aligned to the shifts obtained in this study.

and sudden increase of water coverage at around 40% RH (Dai et al., 1997; Peters et al., 1997; Foster and Ewing, 2000). Kelvin probe microscopy (KPM) experiments by Cabrera-Sanfelix et al. (2007) and Verdaguer et al. (2005, 2008) show how water vapor affects the surface potential of the NaCl(001) surface. They found variations on the order of 0.1 V to 0.25 V across the RH range of their experiments, which clearly is not sufficient to explain the energy shifts. Instead, variations in surface potential will affect the peak broadening as photoelectrons from different areas of the surface feel a different potential and therefore are slightly shifted. The decrease in peak broadening observed for single crystals is ultimately attributed to adsorbed water reducing inhomogeneities in the surface potential. These inhomogeneities originate from potential differences between and within the step and terrace sites of the crystal. The KPM experiments show that the inhomogeneities are removed immediately after water is adsorbed on the surface. In the present work, the deposited NaCl aerosol particle samples are most likely very far from perfect crystals, possibly containing a large number of steps, terraces and kinks leading to larger variations in the surface potential and thus increased broadening of the peaks in any humidity condition. This could, together with the modest experimental resolution, explain why no decrease in the broadening of the peaks is observed for the aerosol particles at low RH.

Considering the relative amounts of Na and Cl on the particle surfaces, we observe a decrease in the Na 1s to Cl 2p peak area ratio, even after taking differences in photoionization cross section and attenuation due to scattering in the water vapor into account. This change as a function of increasing RH is presented in Fig. 4. The extracted Na to Cl ratio of 0.9 at 0% RH is close to the expected stoichiometric ratio of 1. However, when RH is increased to 6.3% and 16%, the ratio clearly decreases to 0.6 and 0.8, respectively. As the spectra for all RH are recorded with a constant excitation energy from the Al Kα anode, different

https://doi.org/10.5194/acp-2020-330
Preprint. Discussion started: 29 April 2020


Atmospheric Chemistry and Physics Discussions

transmission through the electron analyzer at different electron kinetic energies cannot explain this behavior. Due to the constant relative transmission, this could lead only to a constant ratio differing from the stoichiometric ratio. Furthermore, the reported transmission of the analyzer is very nearly the same for the Cl 2p and Na 1s regions (SPECS Surface Nano Analysis GmbH). This correlation between changes in the chemical composition of the surface layer and RH is a clear indication of water being adsorbed to the NaCl particle surfaces. Assuming that the distance of the adsorbed water molecules from the NaCl surface is approximately 2.4 Å (Cabrera-Sanfelix et al., 2007), the photoelectrons emitted from the NaCl surface need to pass through a 2.4 Å thick layer and would be attenuated by collisions with the water molecules in the process. In our experimental conditions, the photoelectrons have kinetic energies (rounded to the nearest ten) of approximately 410 eV and 1290 eV for Na 1s and Cl 2p, respectively. The two core level signals will therefore be attenuated differently due to the different inelastic mean free paths of the electrons, approximately 2 nm and 5 nm, respectively (Emfietzoglou and Moscovitch, 2002).

To quantify the attenuation, we use an exponential decay $I_n = I_n^0 e^{-x/\lambda_n}$, where I_n is the attenuated intensity of peak n, I_n^0 is the unattenuated intensity, x is depth of origin of the signal and λ_n the inelastic mean free path of peak n. Taking the ratio of two peaks, designated 1 and 2, and solving for x, the depth of origin becomes $x = \frac{\lambda_1\lambda_2}{\lambda_1-\lambda_2}\ln R$, where $R = \frac{I_1 I_2^0}{I_2 I_1^0}$ is the relative ratio of the two signals. In the present case ($I_1^0/I_2^0 = 0.9$, measured without water vapor), this simple attenuation model gives depths of photoelectron origin (or water layer thickness) of approximately 1.4 and 0.4 nm for 6.3 and 16% RH, respectively. This is clearly not in line with the previous observations of 2.4 Å and also counterintuitive as it would mean decreasing layer thickness with increasing RH. Furthermore, this simple attenuation model implicitly assumes at least a full monolayer coverage so that all signal is uniformly attenuated by the adsorbed water layer. Previous studies on NaCl (100) crystals (Peters et al., 1997; Peters and Ewing, 1997; Foster and Ewing, 2000) have shown that a full water monolayer does not develop until approximately 35% RH. On the other hand, it has been shown that NaCl (100) does not adsorb water strongly whereas small particles (1-10 μm) have a propensity for adsorbing large amounts of water (Ghosal and Hemminger, 2004). This strong adsorption has also been connected to water remaining on the particle surface, even at elevated temperatures in vacuum. Indeed, this is also observed in the present work in the form of a memory effect in the Na 1s and Cl 2p peak shifts as the humidity is decreased to 0% RH: the peak shift does not completely disappear, even after heating the sample to 125 °C (Fig. S1 in the supplement). The signs of stronger water adsorption in the present work could therefore be attributed to the small size of our sampled NaCl particles, contributing to larger surface area (as well as more crystal imperfections) and therefore to a larger number of possible surface adsorption sites.

While attenuation observed due to the adsorbed water layer is one possible explanation for the decreasing Na to Cl ratio observed in this work, another, complementary, explanation could be the preferential dissolution of Cl^- ions into the water film. Spatial segregation of the Na^+ and Cl^- ions could further enhance the difference in the attenuation between Na 1s and Cl 2p XPS signals. In this case, the Cl 2p photoelectrons only need to pass through part of the water layer while the Na 1s electrons will be attenuated by both a layer of water as well as the dissolved Cl^- ions. This interpretation is supported by density functional theory (DFT) calculations and contact potential measurements (Cabrera-Sanfelix et al., 2007), which showed that Cl^- can indeed be lifted out of a NaCl (100) crystal surface already at one monolayer water coverage.

https://doi.org/10.5194/acp-2020-330
Preprint. Discussion started: 29 April 2020

Atmospheric Chemistry and Physics Discussions

Another possible explanation for the difference in the Na to Cl ratio could be beam damage. Cl has been shown to be more prone to the effect of irradiation, and in the course of the experiments this could mean an accumulating loss of Cl due to desorption or diffusion (Verdaguer et al., 2008). Our results, however, show exactly the opposite: the Cl is enhanced with respect to Na. Furthermore, the radiation from the X-ray anode is far less intense than that produced by a synchrotron, making the effects due to beam damage less likely. This leads us to conclude that the effect cannot be due to beam damage.

The presence of halide ions, especially Cl^- and Br^-, at the air-water interface has been connected to increased photochemical activity (see George and Abbatt (2010) and references therein). Hautala et al. (2017b) found that Br^- ions were closer to the surface that their counter cations in free-flying sub-2 nm CsBr water clusters. Together with the observations presented here, this suggests that nanoscale NaCl aerosol particles have the potential of influencing the atmospheric chemistry already at very low RH conditions.

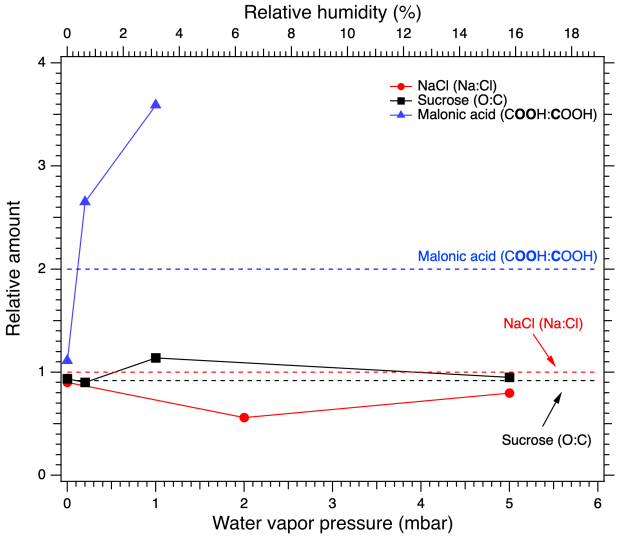

Figure 4. Relative peak areas for NaCl (Na:Cl, red circles), sucrose (O:C, black squares) and malonic acid (C**OO**H:**C**OOH, blue triangles). The dashed horizontal red, black and blue lines show the expected stoichiometric ratio for NaCl, sucrose and malonic acid, respectively. Relative ratios differing from the stoichiometric ratio indicate changes in the chemical composition of the surface of the aerosol particles.

3.2 Sucrose

Figure 5 shows the C 1s XPS spectra of deposited sucrose aerosol particles. The C 1s spectra were fitted with three peaks corresponding to distinct carbon atoms in C-C/C-H, C-O and O-C-O bonds at 285.24, 286.90 and 288.30 eV, respectively, at 0% RH. Sucrose molecules contain only C-O and O-C-O bound carbon and the largest peak corresponding to C-C/C-H bound carbon is therefore attributed to so-called adventitious carbon on the substrate, a thin layer of carbon containing material that forms on samples exposed to ambient air. During fitting of the spectra, the separation between the C-O and O-C-O carbon peaks was fixed to 1.4 eV at all UHV vacuum conditions below 10^{-8} mbar, based on previous XPS studies of disaccharides

https://doi.org/10.5194/acp-2020-330
Preprint. Discussion started: 29 April 2020

Atmospheric Chemistry and Physics Discussions

by Stevens and Schroeder (2009). The fitted C-O and O-C-O peaks were however not linked to the C-C peak, as there are no purely C-C bound carbon in sucrose itself. The intensity ratios of the peaks were left unconstrained during fitting. All peaks were forced to have the same symmetric Voigt line shape, as we expect the line shape to be dominated by the natural broadening of the Mg K_α X-ray emission lines (680 meV) and the instrumental broadening of the electron analyzer (approximately 1000 meV). The obtained peak energies at 0% RH for C-O and O-C-O carbons are in good agreement with values reported by Stevens and Schroeder (2009), 286.7 and 288.1 eV, respectively.

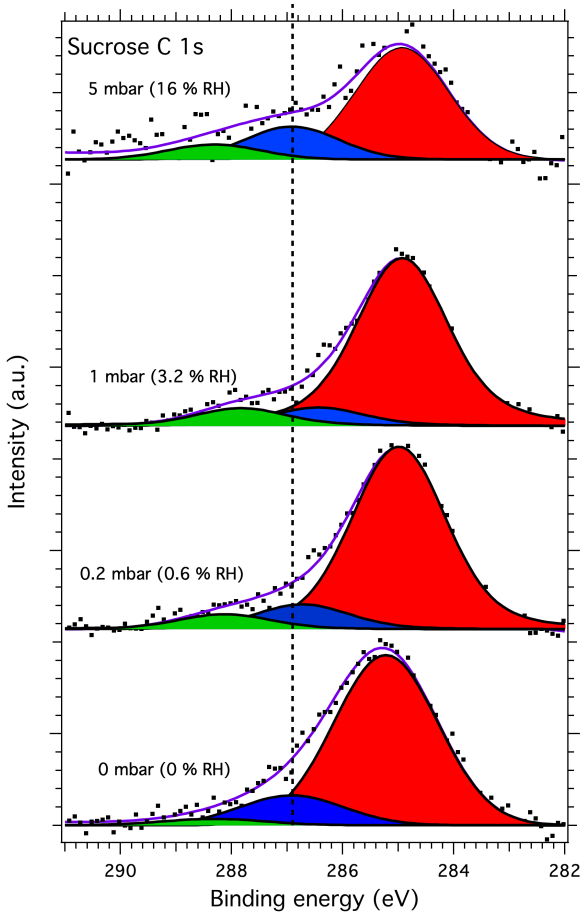

Figure 5. C 1s XPS spectra of sucrose aerosol particles. The dots show the recorded data, the solid lines the fit envelope curve and the red, blue and green peaks the C-C/C-H, C-O and O-C-O bound carbon components, respectively. The dashed vertical line shows the binding energy of the C-O component at 0 mbar pressure (0% RH) at the beginning of the experiments. Photon energy was 1253.6 eV from the Mg anode.

Figure 6 shows the O 1s XPS spectra of the deposited sucrose aerosol particles. The O 1s spectra were fitted with two (C-O and O-C-O bound oxygen) peaks for sucrose and one peak for the water vapor. The separation between the two sucrose C-O and O-C-O oxygen peaks was fixed at 0.7 eV in all humidity conditions (Stevens and Schroeder, 2009). Both peaks were fixed

https://doi.org/10.5194/acp-2020-330
Preprint. Discussion started: 29 April 2020

Atmospheric Chemistry and Physics Discussions

to have the same symmetric line shape. The third peak in the XPS spectra measured in humid conditions is the O 1s signal from the water vapor (Patel et al., 2019), as evidenced by the increase in signal with increasing humidity. The binding energies of the C-O and O-C-O peaks at 0% RH were determined to be 532.39 eV and 533.09, respectively. These values differ slightly from those reported by Stevens and Schroeder (2009) (533.0 eV and 533.7 eV, respectively).

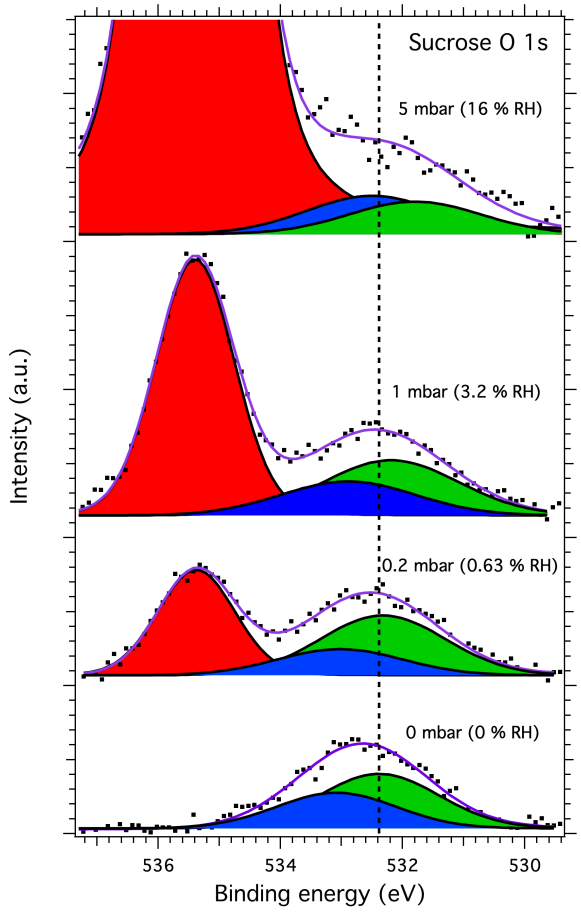

Figure 6. O 1s XPS spectra of sucrose aerosol particles. The dots show the recorded data, the solid lines the fit envelope curve and the red, blue and green peaks the water vapor, and sucrose O-C-O and C-O components, respectively. The dashed vertical line shows the binding energy of the C-O component at 0 mbar pressure (0% relative humidity) at the beginning of the experiments. Photon energy was 1253.6 eV from the Mg anode.

The binding energy shifts of sucrose C 1s and O 1s peaks with respect to 0% RH are shown in Fig. 3 (black squares and diamonds, respectively). Because the peak separation in each case is fixed, only a single shift is reported for spectra of each element. The C 1s shows initially a small shift and then returns to 0 at 16% RH. The O 1s peaks on the other hand seem to shift slightly towards lower binding energies (580 meV at 16% RH). Figure 4 shows the O:C ratio of sucrose as a function of RH. The ratio is in all conditions very close to the stoichiometric value of O:C$= 11/12 \approx 0.92$. Looking specifically at the

https://doi.org/10.5194/acp-2020-330
Preprint. Discussion started: 29 April 2020


Atmospheric Chemistry and Physics Discussions

relative ratios of C-O and O-C-O bound carbon C 1s and oxygen O 1s peaks, we see only minor changes with RH. The C-O C 1s signal seems to increase slightly from 0% to 3.2% RH, but is again lower at 16% RH. The same is seen for the O 1s O-C-O signal, which increases slightly from dry conditions towards 16% RH. Taken together, the observations that both the O 1s and C 1s peaks only show a small binding energy shift with increasing RH, the O:C ratio remains nearly constant and the changes in relative ratios between C-O and O-C-O bound carbon C 1s and oxygen O 1s signals are small, suggest that either there is no significant amounts of water adsorbed onto the particles at RH below 16% or that, if water is adsorbed, there is no significant chemical interaction between the water and the sucrose nanoparticle.

These observations are in line previous results (Zobrist et al., 2011; Yao et al., 2011). Zobrist et al. (2011) used optical techniques to determine the size of single sucrose microparticles levitated in an electrodynamic balance (EDB) under varying RH conditions. Their results show that crystalline sucrose barely adsorbs any water before the deliquescence point of 85.6%. They also show that sucrose does not exhibit any efflorescence upon drying, but instead assumes an amorphous glassy state. On subsequent humidification cycles the amorphous sucrose particle did not show any significant water uptake before RH of 35-40%. It must be kept in mind, however, that the optical detection is a volumetric method and will require much larger amounts of water adsorption to detect changes in particle size. Our present work also supports this observation on the molecular level. In contrast to NaCl particles, the lack of changes in the sucrose C 1s and O 1s binding energies and O to C ratio with increasing RH indicates insignificant water uptake by sucrose aerosol particles at humidities up to 16% RH.

3.3 Malonic Acid

Figures 7 and 8 show the recorded C 1s and O 1s XPS spectra, respectively, of deposited malonic acid aerosol particles at different relative humidities. The C 1s spectra were fitted with three main peaks corresponding to C-C/C-H bound carbon originating from adventitious carbon, COOH and C-C carbon from malonic acid particles at 285.5, 289.8 and 285.8 eV, respectively, in UHV conditions. The adventitious carbon C-C/C-H and the malonic acid COOH peaks were not fixed in energy, whereas the malonic acid C-C peak was fixed at 4.0 eV lower binding energy than the COOH peak. The intensity of the attributed malonic acid C-C peak was fixed to half of that of the COOH peak, reflecting the expected stoichiometry in malonic acid molecules.

Malonic acid has been shown to be prone to beam damage when exposed to radiation from laboratory X-ray sources. This can give rise to additional peaks in the XPS spectra arising from malonic acid molecules damaged by the X-ray beam (Ferreira Jr. et al., 2017a, b). These peaks, denoted DP1 and DP2, following the notation of Ferreira Jr. et al. (2017b) were also included in the fit for 0% RH (UHV), where a good fit could not be produced without their inclusion. They were fixed to be at 1.5 eV (DP1) and 1.2 eV (DP2) higher binding energies than the malonic acid C-C and COOH carbon peaks, respectively. In UHV conditions, the DP1 and DP2 peaks were observed at 291.3 eV and 287.0 eV. The spectra recorded with water vapor did not show clear indication of the DP2 feature, but an additional peak needs to be fitted close to the DP1 feature in both 0.6% and 3.2% RH spectra. This feature was let to vary freely in energy and intensity, but the shape was fixed to be the same as for the other lines in the spectra. The best fit was acquired with the feature at 286.8 eV and 286.2 eV for 0.6% and 3.2% RH, respectively. This is 1.4 eV higher than the C-C carbon peak of malonic acid in both cases, in good agreement with the position of the DP1 peak of Ferreira Jr. et al. (2017b).

https://doi.org/10.5194/acp-2020-330
Preprint. Discussion started: 29 April 2020

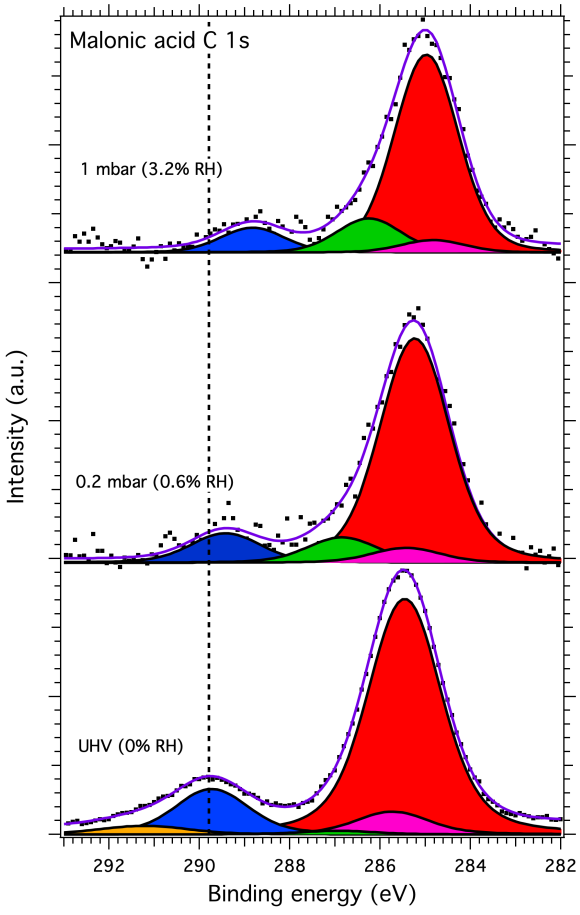

Figure 7. C 1s spectra of malonic acid aerosol particles. The dots show the recorded data and the solid lines the fit to the data. The blue and purple peaks correspond to COOH and C-C of malonic acid, respectively while the yellow and green peaks correspond to DP1 and DP2 components, respectively, from beam damage. The red peak corresponds to C-C/C-H of adventitious carbon. The dashed vertical line shows the binding energy of the COOH component at 0 mbar pressure (0% relative humidity) at the beginning of the experiments. Photon energy was 1253.6 eV from the Mg anode.

The malonic acid O 1s spectra were fitted with two main peaks for the C=O and C-OH bound oxygen of the two carboxyl groups. For UHV conditions, the best fit was acquired with a splitting of approximately 1.0 eV between the C=O and C-OH peaks (at 532.0 and 533.0 eV, respectively). This splitting is smaller than the previously reported values of 1.1 and 1.3 eV by
325 Ferreira Jr. et al. (2017b). For our measurements with water vapor, the best fits were obtained with a splitting of 1.2 eV between the C=O and C-OH oxygen peaks (at 531.6 and 532.8 eV at 3.2% RH, respectively), now in good agreement with the work of Ferreira Jr. et al. (2017b). The peak at highest binding energy in the spectra recorded at humid conditions is the O 1s peak from water vapor. While peaks due to possible beam damage were observed in the C 1s spectra of malonic acid (DP1 and DP2 in Fig. 7), fitting corresponding peaks in the O 1s spectrum did not yield a better representation of the measured XPS spectra.

https://doi.org/10.5194/acp-2020-330
Preprint. Discussion started: 29 April 2020

Atmospheric Chemistry and Physics Discussions

However, this is in line with the previous works of Ferreira Jr. et al. (2017a), showing that the signal due to beam damage is much less pronounced in the O 1s spectra than in the C 1s spectra.

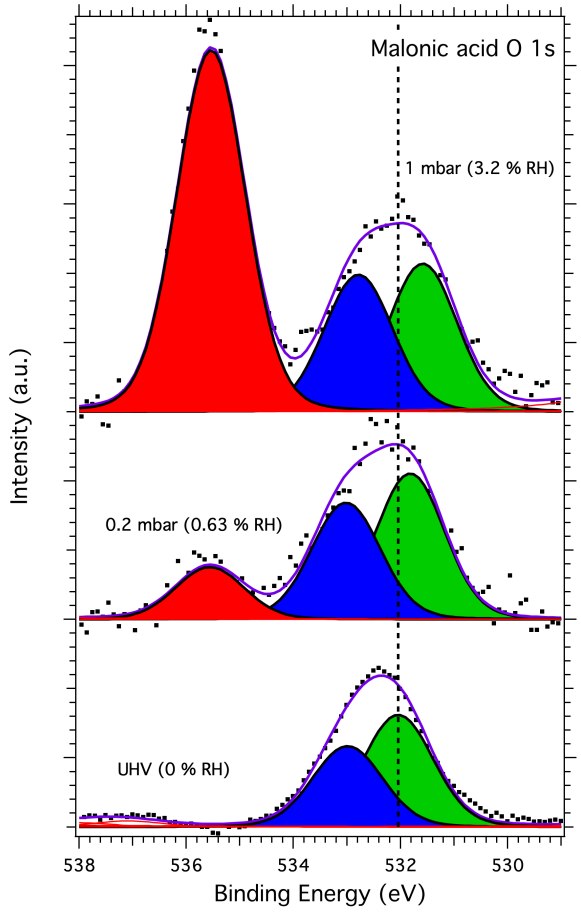

Figure 8. O 1s spectra of malonic acid aerosol particles. The dots show the recorded data, the solid lines the fit envelope curve and the red, blue and green peaks the water vapor, C-OH and C=O components, respectively. The dashed vertical line shows the binding energy of the C=O component at 0 mbar pressure (0% relative humidity) at the beginning of the experiments. Photon energy was 1253.6 eV from the Mg anode.

The binding energy shifts of malonic acid particle C 1s and O 1s peaks with respect to 0% RH are shown in Fig. 3 (blue triangles and diamonds, respectively). When RH is increased, the COOH (and thus also C-C) peaks of malonic acid are seen to shift towards lower binding energies. While the the shift for malonic acid O 1s is not as dramatic as for NaCl particles, the malonic acid C 1s binding energies shift is even more pronounced than that of Na 1s or Cl 2p, indicating that water is being adsorbed onto the surface of the malonic acid particles, changing the chemical environment of the surface molecules. In addition to the peaks shifts, the C 1s to O 1s signal ratio (O(COOH):C(COOH)) within the malonic acid carboxyl group changes with increasing RH. We focus on the ratio O(COOH):C(COOH), as the C-C/C-H contribution is under the strong

https://doi.org/10.5194/acp-2020-330
Preprint. Discussion started: 29 April 2020


Atmospheric Chemistry and Physics Discussions

C-C/C-H signal from adventitious carbon and therefore cannot be fitted reliably. The stoichiometric O:C ratio of a carboxyl group is 2. Interestingly, already at 0% RH (UHV), the extracted ratio O(COOH):C(COOH)= 1.2 is far from this stoichiometric value. When introducing water vapor into the system at 0.6% RH, the ratio changes to 2.4. At 3% RH, it increases even further to O(COOH):C(COOH)= 3.1. While we cannot offer a clear explanation for this observation at the present, based on the observed binding energy shifts and the changes in the O(COOH):C(COOH) ratio, it is safe to conclude that water is adsorbed on nanoscale malonic acid aerosols particles already at the lowest RH measured and that it has an effect on the chemical composition of the particle surface.

On closer inspection of the malonic acid spectra, it is clear that the C 1s spectrum at 0% RH (UHV) resembles that of a beam damaged sample described by Ferreira Jr. et al. (2017a, b), but not entirely: the DP2 feature in our particle spectra is stronger than reported by Ferreira Jr. et al. (2017b) and the DP1 weaker. When increasing the RH in our measurements, the stronger DP2 peak disappears and only the extra feature attributed to DP1 is seen. Our malonic acid particle O 1s spectra do not show any signs of beam damage even at increased RH. Instead, the relative intensities between the C=O and C-OH components change towards the expected (C=O:C-OH) ratio of 1 from the C=O:C-OH = 1.4 observed at 0% RH (UHV). This indicates an increase in the number of C-OH and decrease in the number of C=O groups on the malonic acid particle surface with increasing RH. Indeed, the binding energy of the C 1s extra (DP2) feature is close to the typical binding energy (approximately 286.5 eV) of a hydroxyl group carbon, C-OH. If this were purely a result of beam damage, the DP2 feature in the C 1s spectrum should also be visible, not to mention the beam damage component in the O 1s spectra. It could therefore be a sign of significant chemical changes in the malonic acid particles.

Malonic acid is known to exhibit keto-enol tautomerism and it has been theoretically predicted that the transition between the two forms can take place through an intramolecular transition in a system of just six water molecules and one malonic acid molecule (see e.g. Yamabe et al. (2004)). Ghorai et al. (2011) performed spectromicroscopic experiments combining scanning transmission X-ray microscopy with near-edge X-ray absorption fine structure spectroscopy (STXM/NEXAFS) and Fourier transform infrared spectroscopy (FTIR) on deliquesced submicron malonic acid aerosol particles at varying RH up to 90%. Their bulk-sensitive experiments show that while the keto form dominates in dilute aqueous solutions of malonic acid, the equilibrium shifts toward the enol form in saturated solutions. This observation is also supported by the theoretical calculations of Dick-Pérez and Windus (2017) for concentrated malonic acid solution particles. The results of Ghorai et al. (2011) show that the amount of enol form increases with increasing relative humidity as water is absorbed by deliquesced malonic acid aerosols. Furthermore, they demonstrate water uptake by malonic acid aerosols already at RH as low as 2%, which is in good agreement with the conclusion of our surface-sensitive XPS experiments in the present work.

The single particle carbon K-edge NEXAFS spectra of Ghorai et al. (2011) show a clear increase in C=C and C-OH resonances, while C-COOH and C-CH are decreased with increasing RH. Their oxygen K-edge spectra also shows a clear decrease in the -COOH resonance. This is similar to the observations of the present work, where the O 1s C-OH signal from malonic acid particle surfaces increases with increasing RH. While a similar increase is observed also in the C 1s for the C-OH (DP1) component, added caution is necessary when attributing this to the enol form of malonic acid. The C-OH peak at approximately 286.5 eV is a sign of carbon with a single hydroxyl group, while the malonic acid enol form would have a carbon with two

https://doi.org/10.5194/acp-2020-330
Preprint. Discussion started: 29 April 2020


Atmospheric Chemistry and Physics Discussions

hydroxyl groups bound to it (HO-C-OH or O-C-O), increasing the binding energy from 286.5 eV to approximately 288 eV. Although no such peak has been fit to the data in the present work, it also cannot be ruled out completely. However, if the spectral changes observed in our XPS experiments are due to the formation of the enol tautomer on the malonic acid particle surface, this could have profound implications in terms of atmospheric chemistry as the keto and enol forms have differing physical and chemical stabilities and reaction pathways in both the gas and aqueous phases (Yamabe et al., 2004).

4 Conclusions

We studied water uptake onto NaCl, sucrose and malonic acid aerosol particles deposited on silicon and gold substrates using the APXPS technique with a laboratory X-ray source (Al Kα and Mg Kα). To our knowledge, this is the first time surface-sensitive and chemically-specific XPS has been used in AP conditions on nano-scale particles of immediate atmospherically relevant compositions.

The samples were exposed to relative humidities between 0% and 16% at room temperature and the XPS spectra of Na 1s, Cl 2p, C 1s and O 1s core levels were recorded. The results show that water is already adsorbed onto the aerosol particles at the very low relative humidities. Corresponding changes were observed in the chemical environment, and possibly even composition, of the particle surfaces with increasing relative humidity. For NaCl particles, we find signs of Cl^- ions dissolving into the thin surface water layer, as well as a memory effect in binding energies when drying back to 0% RH. This water uptake memory persists even after heating the particles up to 125 °C. Although some water seems to remain on the particles, the Cl appears to return to the crystal lattice of the aerosol as the particle is dried. Sucrose particles show very little changes when exposed to water vapor at the conditions of these experiments. Malonic acid particles on the other hand show a dramatic shift in the C 1s binding energies even when exposed to very small amounts of water (0.2–3% RH), as well as a shift in the O 1s binding energies. Changes are also seen in the relative amounts of C=O and C-OH bound oxygen on the surface of malonic acid particles, together with the emergence of C-OH bound carbon at the cost of COOH. These surface specific changes are in line with earlier bulk-sensitive observations of water uptake by malonic acid particles at very low RH (Ghorai et al., 2011) and could even indicate a change in the keto-enol equilibrium of malonic acid within the surface adsorbed water layer in our experiments.

The present observations suggest that while sucrose particles do not interact appreciably with water vapor at low RH conditions, the adsorption of small amounts of water onto NaCl and malonic acid particles could already have implications for atmospheric chemistry on a molecular level. For example, Cl^- ions in sea salt aerosols are a source of chlorine in the troposphere through heterogeneous conversion to chlorines and chlorides (see e.g. Wang et al. (2019) and references therein). With sea salt being one of the most abundant inorganic aerosol components in the global atmosphere, our present observations could imply significant reactive uptake and processing of atmospheric trace gases even at low RH. Dicarboxylic acids like malonic acid are also ubiquitous in atmospheric aerosols in the troposphere. The formation of concentrated solutions with the enol form present even in relatively dry conditions may have important implications for the reactivity of these aerosol surfaces. The role of particle surfaces is enhanced for smaller particles with large surface-to-bulk ratios (Prisle et al., 2012; Bzdek et al., 2020).

https://doi.org/10.5194/acp-2020-330
Preprint. Discussion started: 29 April 2020


Atmospheric Chemistry and Physics Discussions

The effects of water uptake detected at very low relative humidities in this work could not have been detected with standard mass or volume based aerosol techniques, nor attributed specifically to the surface with bulk sensitive spectroscopic methods.

Our results demonstrate the viability of the APXPS technique for *in situ* studies of vapor interaction with aerosol particle surfaces. XPS can provide surface-specific, molecular-level chemical information on uptake and reactions through changes in the presence, position or intensity of spectral peaks. We have shown that APXPS can be used on sampled aerosol particles comprising both organic and inorganic components of high atmospheric relevance. Our samples were generated with standard aerosol laboratory methods and exposed to a well-defined vapor phase during experiments. Our experiments were carried out using a conventional laboratory X-ray source. Combining APXPS with high brilliance synchrotron radiation now available at modern synchrotron facilities therefore shows great promise for studying aerosol surfaces at even higher pressure conditions, more reactive environments as well as with high time resolution.

Author contributions. Conceptualization: NLP; Funding acquisition: NLP; Analysis: JJL, SW, SU, and NLP; Investigation: JJL, KRR, SW, EK, M-HM, and SU; Project administration: NLP; Supervision: SU and NLP; Visualization: SU; Writing: JJL, SU, and NLP with input from all co-authors

Competing interests. The authors declare that they have no conflict of interest.

Acknowledgements. This project has received funding from the European Research Council (ERC) under the European Union's Horizon 2020 research and innovation programme, Project SURFACE (Grant Agreement No. 717022). The authors also gratefully acknowledge the financial contribution from the Academy of Finland, including Grant Nos. 308238, 314175, 290145, and 326291. We acknowledge MAX IV Laboratory for time on Beamline SPECIES. Research conducted at MAX IV, a Swedish national user facility, is supported by the Swedish Research council under contract 2018-07152, the Swedish Governmental Agency for Innovation Systems under contract 2018-04969, and Formas under contract 2019-02496. We warmly thank Jenny Rissler and Birgitta Svenningsson for assistance with preparation of samples and estimation of surface coverage.

https://doi.org/10.5194/acp-2020-330
Preprint. Discussion started: 29 April 2020

Atmospheric Chemistry and Physics Discussions

References

Ammann, M., Artiglia, L., and Bartels-Rausch, T.: X-Ray Excited Electron Spectroscopy to Study Gas–Liquid Interfaces of Atmospheric Relevance, in: Physical Chemistry of Gas-Liquid Interfaces, pp. 135–166, Elsevier, 2018.

Antonsson, E., Patanen, M., Nicolas, C., Neville, J. J., Benkoula, S., Goel, A., and Miron, C.: Complete Bromide Surface Segregation in Mixed NaCl/NaBrAerosols Grown from Droplets, Physical Review X, 5, 011 025–7, 2015.

Ault, A. P. and Axson, J. L.: Atmospheric Aerosol Chemistry: Spectroscopic and Microscopic Advances, Analytical Chemistry, 89, 430–452, 2016.

Bilde, M. and Svenningsson, B.: CCN activation of slightly soluble organics: the importance of small amounts of inorganic salt and particle phase, Tellus B, 56, 128–134, 2004.

Boucher, O., Randall, D., Artaxo, P., Bretherton, C., Feingold, G., Forster, P., Kerminen, V.-M., Kondo, Y., Liao, H., Lohmann, U., Rasch, P., Satheesh, S., Sherwood, S., Stevens, B., and Zhang, X.: Clouds and Aerosols. In: *Climate Change 2013: The Physical Science Basis. Contribution of Working Group I to the Fifth Assessment Report of the Intergovernmental Panel on Climate Change* [Stocker, T.F., D. Qin, G.-K. Plattner, M. Tignor, S.K. Allen, J. Boschung, A. Nauels, Y. Xia, V. Bex, and P.M. Midgley (eds.)]., Cambridge University Press, Cambridge, United Kingdom and New York, NY, USA, 2013.

Bzdek, B. R., Reid, J. P., Malila, J., and Prisle, N. L.: The surface tension of surfactant-containing, finite volume droplets, Proceedings of the National Academy of Sciences, 39, 201915 660, 2020.

Cabrera-Sanfelix, P., Sanchez Portal, D., Verdaguer, A., Darling, G. R., Salmeron, M., and Arnau, A.: Spontaneous Emergence of Cl -Anions from NaCl(100) at Low Relative Humidity, The Journal of Physical Chemistry C, 111, 8000–8004, 2007.

Cwiertny, D. M., Young, M. A., and Grassian, V. H.: Chemistry and Photochemistry of Mineral Dust Aerosol, Annual Review of Physical Chemistry, 59, 27–51, 2008.

Dai, Q., Hu, J., and Salmeron, M.: Adsorption of Water on NaCl (100) Surfaces: Role of Atomic Steps, The Journal of Physical Chemistry B, 101, 1994–1998, 1997.

Decesari, S., Facchini, M. C., Fuzzi, S., and Tagliavini, E.: Characterization of water-soluble organic compounds in atmospheric aerosol: A new approach, Journal of Geophysical Research, 105, 1481–1489, 2000.

Decesari, S., Facchini, M. C., Matta, E., Lettini, F., Mircea, M., Fuzzi, S., Tagliavini, E., and Putaud, J. P.: Chemical features and seasonal variation of fine aerosol water-soluble organic compounds in the Po Valley, Italy, Atmospheric Environment, 35, 3691–3699, 2001.

Dick-Pérez, M. and Windus, T. L.: Computational Study of the Malonic Acid Tautomerization Products in Highly Concentrated Particles, The Journal of Physical Chemistry A, 121, 2259–2264, 2017.

Emfietzoglou, D. and Moscovitch, M.: Inelastic collision characteristics of electrons in liquid water, Nuclear Instruments and Methods in Physics Research Section B: Beam Interactions with Materials and Atoms, 193, 71–78, 2002.

Estillore, A. D., Morris, H. S., Or, V. W., Lee, H. D., Alves, M. R., Marciano, M. A., Laskina, O., Qin, Z., Tivanski, A. V., and Grassian, V. H.: Linking hygroscopicity and the surface microstructure of model inorganic salts, simple and complex carbohydrates, and authentic sea spray aerosol particles, Physical Chemistry Chemical Physics, 19, 21 101–21 111, 2017.

Ferreira Jr., J. M., Trindade, G. F., Tshulu, R., Watts, J. F., and Baker, M. A.: Introduction to a series of dicarboxylic acids analyzed by x-ray photoelectron spectroscopy, Surface Science Spectra, 24, 011 001–5, 2017a.

Ferreira Jr., J. M., Trindade, G. F., Tshulu, R., Watts, J. F., and Baker, M. A.: Dicarboxylic acids analysed by x-ray photoelectron spectroscopy, Part I - propanedioic acid anhydrous, Surface Science Spectra, 24, 011 101–8, 2017b.

https://doi.org/10.5194/acp-2020-330
Preprint. Discussion started: 29 April 2020

Atmospheric Chemistry and Physics Discussions

Foster, M. C. and Ewing, G. E.: Adsorption of water on the NaCl(001) surface. II. An infrared study at ambient temperatures, The Journal of Chemical Physics, 112, 6817–6826, 2000.

Freedman, M. A., Ott, E.-J. E., and Marak, K. E.: Role of pH in Aerosol Processes and Measurement Challenges, The Journal of Physical Chemistry A, 123, 1275–1284, 2018.

George, I. J. and Abbatt, J. P. D.: Heterogeneous oxidation of atmospheric aerosolparticles by gas-phase radicals, Nature Publishing Group, 2, 713–722, 2010.

Ghorai, S., Laskin, A., and Tivanski, A. V.: Spectroscopic Evidence of Keto–Enol Tautomerism in Deliquesced Malonic Acid Particles, The Journal of Physical Chemistry A, 115, 4373–4380, 2011.

Ghosal, S. and Hemminger, J. C.: Surface Adsorbed Water on NaCl and Its Effect on Nitric Acid Reactivity with NaCl Powders, The Journal of Physical Chemistry B, 108, 14 102–14 108, 2004.

Hautala, L., Jänkälä, K., Löytynoja, T., Mikkelä, M. H., Prisle, N., Tchaplyguine, M., and Huttula, M.: Experimental observation of structural phase transition in CsBr clusters, Physical Review B, 95, 045 402, 2017a.

Hautala, L., Jänkälä, K., Mikkelä, M.-H., Turunen, P., Prisle, N. L., Patanen, M., Tchaplyguine, M., and Huttula, M.: Probing RbBr solvation in freestanding sub-2 nm water clusters, Physical Chemistry Chemical Physics, 19, 25 158–25 167, 2017b.

Herrmann, H., Hoffmann, D., Schaefer, T., Bräuer, P., and Tilgner, A.: Tropospheric Aqueous-Phase Free-Radical Chemistry: Radical Sources, Spectra, Reaction Kinetics and Prediction Tools, ChemPhysChem, 11, 3796–3822, 2010.

Hori, M., Ohta, S., Murao, N., and Yamagata, S.: Activation capability of water soluble organic substances as CCN, Journal of Aerosol Science, 34, 419–448, 2003.

Kanakidou, M., Seinfeld, J. H., Pandis, S. N., Barnes, I., Dentener, F. J., Facchini, M. C., Van Dingenen, R., Ervens, B., Nenes, A., Nielsen, C. J., Swietlicki, E., Putaud, J. P., Balkanski, Y., Fuzzi, S., Horth, J., Moortgat, G. K., Winterhalter, R., Myhre, C. E. L., Tsigaridis, K., Vignati, E., Stephanou, E. G., and Wilson, J.: Organic aerosol and global climate modelling: a review, Atmospheric Chemistry and Physics, 5, 1053–1123, 2005.

Khwaja, H. A.: Atmospheric concentrations of carboxylic acids and related compounds at a semiurban site, Atmospheric Environment, 29, 127–139, 1995.

Knudsen, J., Andersen, J. N., and Schnadt, J.: A versatile instrument for ambient pressure x-ray photoelectron spectroscopy: The Lund cell approach, Surface Science, 646, 160–169, 2016.

Kong, X., Castarède, D., Boucly, A., Artiglia, L., Ammann, M., Bartels-Rausch, T., Thomson, E. S., and Pettersson, J. B. C.: Reversibly Physisorbed and Chemisorbed Water on Carboxylic Salt Surfaces Under Atmospheric Conditions, The Journal of Physical Chemistry C, 124, 5263–5269, 2020.

Kreidenweis, S. M. and Asa-Awuku, A.: Aerosol Hygroscopicity: Particle Water Content and Its Role in Atmospheric Processes, in: Treatise on Geochemistry, edited by Holland, H. D. and Turekian, K. K., pp. 331–361, Elsevier, Oxford, 2014.

Kukk, E., Snell, G., Bozek, J. D., Cheng, W. T., and Berrah, N.: Vibrational structure and partial rates of resonant Auger decay of the $\mathrm{N}\,1s \rightarrow 2\pi$ core excitations in nitric oxide, Physical Review A, 63, 143–9, 2001.

Kukk, E., Ueda, K., Hergenhahn, U., Liu, X. J., Prümper, G., Yoshida, H., Tamenori, Y., Makochekanwa, C., Tanaka, T., Kitajima, M., and Tanaka, H.: Violation of the Franck-Condon Principle due to Recoil Effects in High Energy Molecular Core-Level Photoionization, Physical Review Letters, 95, 133 001–4, 2005.

https://doi.org/10.5194/acp-2020-330
Preprint. Discussion started: 29 April 2020

Atmospheric Chemistry and Physics Discussions

Lampimäki, M., Schreiber, S., Zelenay, V., Křepelová, A., Birrer, M., Axnanda, S., Mao, B., Liu, Z., Bluhm, H., and Ammann, M.: Exploring the Environmental Photochemistry on the TiO 2(110) Surface in Situ by Near Ambient Pressure X-ray Photoelectron Spectroscopy, The Journal of Physical Chemistry C, 119, 7076–7085, 2015.

Laskin, A., Moffet, R. C., Gilles, M. K., Fast, J. D., Zaveri, R. A., Wang, B., Nigge, P., and Shutthanandan, J.: Tropospheric chemistry of internally mixed sea salt and organic particles: Surprising reactivity of NaCl with weak organic acids, Journal of Geophysical Research, 117, n/a–n/a, 2012.

McNeill, V. F.: Aqueous Organic Chemistry in the Atmosphere: Sources and Chemical Processing of Organic Aerosols, Environmental Science & Technology, 49, 1237–1244, 2015.

Muñoz, A., Oller, J. C., Blanco, F., Gorfinkiel, J. D., Limão-Vieira, P., and García, G.: Electron-scattering cross sections and stopping powers in H2O, Physical Review A, 76, 707–7, 2007.

Murphy, D. M., Froyd, K. D., Bian, H., Brock, C. A., Dibb, J. E., DiGangi, J. P., Diskin, G., Dollner, M., Kupc, A., Scheuer, E. M., Schill, G. P., Weinzierl, B., Williamson, C. J., and Yu, P.: The distribution of sea-salt aerosol in the global troposphere, Atmospheric Chemistry and Physics, 19, 4093–4104, 2019.

Newberg, J. T., Starr, D. E., Yamamoto, S., Kaya, S., Kendelewicz, T., Mysak, E. R., Porsgaard, S., Salmeron, M. B., Brown Jr., G. E., Nilsson, A., and Bluhm, H.: Autocatalytic Surface Hydroxylation of MgO(100) Terrace Sites Observed under Ambient Conditions, The Journal of Physical Chemistry C, 115, 12 864–12 872, 2011.

Nguyen, T. K. V., Zhang, Q., Jimenez, J. L., Pike, M., and Carlton, A. G.: Liquid Water: Ubiquitous Contributor to Aerosol Mass, Environmental Science & Technology Letters, p. acs.estlett.6b00167, 2016.

Ogletree, D. F., Bluhm, H., Hebenstreit, E. L. D., and Salmeron, M.: Photoelectron spectroscopy under ambient pressure and temperature conditions, Nuclear Instruments and Methods in Physics Research Section A: Accelerators, Spectrometers, Detectors and Associated Equipment, 601, 151–160, 2009.

Ouf, F. X., Parent, P., Laffon, C., Marhaba, I., Ferry, D., Marcillaud, B., Antonsson, E., Benkoula, S., Liu, X. J., Nicolas, C., Robert, E., Patanen, M., Barreda, F. A., Sublemontier, O., Coppalle, A., Yon, J., Miserque, F., Mostefaoui, T., Regier, T. Z., Mitchell, J. B. A., and Miron, C.: First in-flight synchrotron X-ray absorption and photoemission study of carbon soot nanoparticles, Nature Publishing Group, 6, 1–12, 2016.

Parsons, M. T., Mak, J., Lipetz, S. R., and Bertram, A. K.: Deliquescence of malonic, succinic, glutaric, and adipic acid particles, Journal of Geophysical Research, 109, n/a–n/a, 2004.

Patel, D. I., Shah, D., Bahr, S., Dietrich, P., Meyer, M., Thißen, A., and Linford, M. R.: Water vapor, by near-ambient pressure XPS, Surface Science Spectra, 26, 014 026–6, 2019.

Peters, S. J. and Ewing, G. E.: Water on Salt: An Infrared Study of Adsorbed H 2O on NaCl(100) under Ambient Conditions, The Journal of Physical Chemistry B, 101, 10 880–10 886, 1997.

Peters, S. J., Langmuir, G. E., and 1997: Thin film water on NaCl (100) under ambient conditions: An infrared study, ACS Publications, 13, 1997.

Pope, F. D., Dennis-Smither, B. J., Griffiths, P. T., Clegg, S. L., and Cox, R. A.: Studies of Single Aerosol Particles Containing Malonic Acid, Glutaric Acid, and Their Mixtures with Sodium Chloride. I. Hygroscopic Growth, The Journal of Physical Chemistry A, 114, 5335–5341, 2010.

Preger, C., Overgaard, N. C., Messing, M. E., and Magnusson, M. H.: Predicting the deposition spot radius and the nanoparticle concentration distribution in an electrostatic precipitator, Aerosol Science and Technology, 1, 1–11, 2020.

https://doi.org/10.5194/acp-2020-330
Preprint. Discussion started: 29 April 2020

Prenni, A. J., DeMott, P. J., Kreidenweis, S. M., Sherman, D. E., Russell, L. M., and Ming, Y.: The Effects of Low Molecular Weight Dicarboxylic Acids on Cloud Formation, The Journal of Physical Chemistry A, 105, 11 240–11 248, 2001.

Prisle, N. L., Ottosson, N., Öhrwall, G., Söderström, J., Dal Maso, M., and Björneholm, O.: Surface/bulk partitioning and acid/base speciation of aqueous decanoate: direct observations and atmospheric implications, Atmospheric Chemistry and Physics, 12, 12 227–12 242, 2012.

Rissman, T. A., Varutbangkul, V., Surratt, J. D., Topping, D. O., McFiggans, G., Flagan, R. C., and Seinfeld, J. H.: Cloud condensation nucleus (CCN) behavior of organic aerosol particles generated by atomization of water and methanol solutions, Atmospheric Chemistry and Physics, 7, 2949–2971, 2007.

Rood, M. J., Shaw, M. A., Larson, T. V., and Covert, D. S.: Ubiquitous nature of ambient metastable aerosol, Nature, 337, 537–539, 1989.

Rossi, M. J.: Heterogeneous Reactions on Salts, Chemical Reviews, 103, 4823–4882, 2003.

Salmeron, M. and Schlögl, R.: Ambient pressure photoelectron spectroscopy: A new tool for surface science and nanotechnology, Surface Science Reports, 63, 169–199, 2008.

Schnadt, J., Knudsen, J., Andersen, J. N., Siegbahn, H., Pietzsch, A., Hennies, F., Johansson, N., Mårtensson, N., Öhrwall, G., Bahr, S., Mahl, S., and Schaff, O.: The new ambient-pressure X-ray photoelectron spectroscopy instrument at MAX-lab, J. Synchrotron Rad (2012). 19, 701-704 [doi:10.1107/S0909049512032700], 19, 1–4, 2012.

Shakya, K. M., Liu, S., Takahama, S., Russell, L. M., Keutsch, F. N., Galloway, M. M., Shilling, J. E., Hiranuma, N., Song, C., Kim, H., Paulson, S. E., Pfaffenberger, L., Barmet, P., Slowik, J., Prévôt, A. S. H., Dommen, J., and Baltensperger, U.: Similarities in STXM-NEXAFS Spectra of Atmospheric Particles and Secondary Organic Aerosol Generated from Glyoxal, α-Pinene, Isoprene, 1,2,4-Trimethylbenzene, and d-Limonene , 2016.

SPECS Surface Nano Analysis GmbH: Calculated Transmission for PHOIBOS NAP 150 R2, https://www.specs-group.com/fileadmin/user_upload/products/technical-note/TNote-PHOIBOS_150_NAP_Calculated_Transmission_function.pdf, accessed: 2020-04-18.

Starr, D. E., Liu, Z., Hävecker, M., Knop-Gericke, A., and Bluhm, H.: Investigation of solid/vapor interfaces using ambient pressure X-ray photoelectron spectroscopy, Chemical Society Reviews, 42, 5833–25, 2013.

Stevens, J. S. and Schroeder, S. L. M.: Quantitative analysis of saccharides by X-ray photoelectron spectroscopy, Surface and Interface Analysis, 41, 453–462, 2009.

Tang, I. N. and Munkelwitz, H. R.: Composition and temperature dependence of the deliquescence properties of hygroscopic aerosols, Atmospheric Environment. Part A. General Topics, 27, 467–473, 1993.

Tang, M., Chan, C. K., Li, Y. J., Su, H., Ma, Q., Wu, Z., Zhang, G., Wang, Z., Ge, M., Hu, M., He, H., and Wang, X.: A review of experimental techniques for aerosol hygroscopicity studies, Atmospheric Chemistry and Physics, 19, 12 631–12 686, 2019.

Toribio, A. R., Prisle, N. L., and Wexler, A. S.: Statistical Mechanics of Multilayer Sorption: Surface Concentration Modeling and XPS Measurement, The Journal of Physical Chemistry Letters, 9, 1461–1464, 2018.

Urpelainen, S., Såthe, C., Grizolli, W., Agåker, M., Head, A. R., Andersson, M., Huang, S.-W., Jensen, B. N., Wallén, E., Tarawneh, H., Sankari, R., Nyholm, R., Lindberg, M., Sjöblom, P., Johansson, N., Reinecke, B. N., Arman, M. A., Merte, L. R., Knudsen, J., Schnadt, J., Andersen, J. N., and Hennies, F.: The SPECIES beamline at the MAX IV Laboratory: a facility for soft X-ray RIXS and APXPS, Journal of Synchrotron Radiation, 24, 344–353, 2017.

Verdaguer, A., Sacha, G. M., Luna, M., Ogletree, D. F., and Salmeron, M.: Initial stages of water adsorption on NaCl (100) studied by scanning polarization force microscopy, The Journal of Chemical Physics, 123, 124 703–9, 2005.

https://doi.org/10.5194/acp-2020-330
Preprint. Discussion started: 29 April 2020

Atmospheric Chemistry and Physics Discussions

Verdaguer, A., Segura, J. J., Fraxedas, J., Bluhm, H., and Salmeron, M.: Correlation between Charge State of Insulating NaCl Surfaces and Ionic Mobility Induced by Water Adsorption: A Combined Ambient Pressure X-ray Photoelectron Spectroscopy and Scanning Force Microscopy Study, The Journal of Physical Chemistry C, 112, 16 898–16 901, 2008.

Walz, M. M., Caleman, C., Werner, J., Ekholm, V., Lundberg, D., Prisle, N. L., Öhrwall, G., and Björneholm, O.: Surface behavior of amphiphiles in aqueous solution: a comparison between different pentanol isomers, Physical Chemistry Chemical Physics, 17, 14 036–14 044, 2015.

Walz, M. M., Werner, J., Ekholm, V., Prisle, N. L., Öhrwall, G., and Björneholm, O.: Alcohols at the aqueous surface: chain length and isomer effects, Physical Chemistry Chemical Physics, 18, 6648–6656, 2016.

Wang, X., Jacob, D. J., Eastham, S. D., Sulprizio, M. P., Zhu, L., Chen, Q., Alexander, B., Sherwen, T., Evans, M. J., Lee, B. H., Haskins, J. D., Lopez-Hilfiker, F. D., Thornton, J. A., Huey, G. L., and Liao, H.: The role of chlorine in global tropospheric chemistry, Atmospheric Chemistry and Physics, 19, 3981–4003, 2019.

Werner, F., Ditas, F., Siebert, H., Simmel, M., Wehner, B., Pilewskie, P., Schmeissner, T., Shaw, R. A., Hartmann, S., Wex, H., Roberts, G. C., and Wendisch, M.: Twomey effect observed from collocated microphysical and remote sensing measurements over shallow cumulus, Journal of Geophysical Research: Atmospheres, 119, 1534–1545, 2014.

Werner, J., Persson, I., Björneholm, O., Kawecki, D., Saak, C.-M., Walz, M.-M., Ekholm, V., Unger, I., Valtl, C., Caleman, C., Öhrwall, G., and Prisle, N. L.: Shifted equilibria of organic acids and bases in the aqueous surface region, Physical Chemistry Chemical Physics, 20, 23 281–23 293, 2018.

Winter, B.: Liquid microjet for photoelectron spectroscopy, Nuclear Instruments and Methods in Physics Research Section A: Accelerators, Spectrometers, Detectors and Associated Equipment, 601, 139–150, 2009.

Yamabe, S., Tsuchida, N., and Miyajima, K.: Reaction Paths of Keto−Enol Tautomerization of β-Diketones, The Journal of Physical Chemistry A, 108, 2750–2757, 2004.

Yao, W., Yu, X., Lee, J. W., Yuan, X., and Schmidt, S. J.: Measuring the Deliquescence Point of Crystalline Sucrose as a Function of Temperature Using a New Automatic Isotherm Generator, International Journal of Food Properties, 14, 882–893, 2011.

Yeh, J. J. and Lindau, I.: Atomic subshell photoionization cross sections and asymmetry parameters: $1 \leqslant Z \leqslant 103$, Atomic Data and Nuclear Data Tables, 32, 1–155, 1985.

Yu, L. E., Shulman, M. L., Kopperud, R., and Hildemann, L. M.: Characterization of Organic Compounds Collected during Southeastern Aerosol and Visibility Study: Water-Soluble Organic Species, Environmental Science & Technology, 39, 707–715, 2005.

Zobrist, B., Soonsin, V., Luo, B. P., Krieger, U. K., Marcolli, C., Peter, T., and Koop, T.: Ultra-slow water diffusion in aqueous sucrose glasses, Physical Chemistry Chemical Physics, 13, 3514–13, 2011.